Combined amperometric/potentiometric probes for improved chemical imaging of corroding surfaces using Scanning Electrochemical Microscopy

D. Filotás[1,2], B.M. Fernández-Pérez[3], J. Izquierdo[3,4], L. Nagy[1,2], G. Nagy[1,2], R.M. Souto[3,4]

[1] *Department for General and Physical Chemistry, Faculty of Sciences, University of Pécs, Ifjúság útja 6, 7624 Pécs, Hungary.*
[2] *János Szentágothai Research Center, University of Pécs, Ifjúság u.20. Pécs, 7624 Hungary.*
[3] *Department of Chemistry, Universidad de La Laguna, P.O. Box 456, E-38200 La Laguna, Tenerife, Canary Islands, Spain.*
[4] *Institute of Material Science and Nanotechnology, Universidad de La Laguna, E-38200 La Laguna (Tenerife), Spain.*

Abstract

Chemical visualization of corrosion processes using scanning electrochemical microscopy (SECM) in combined amperometric/potentiometric operation has been achieved by developing novel multi-barrel probes as tips. A Pt-based amperometric disc probe is employed for the detection and characterization of reactive sites on a corroding system, whereas a Sb-based disc microelectrode is employed to visualize local solution pH changes. Quasi-simultaneous imaging of localized corrosion micro-cells on the surface and the associated pH variations in the electrolyte, resulting from both the electrolysis of dissolved metal ions from the local anodes and the consumption of an oxidizing agent at the local cathodes, can be obtained in the same solution without changing the probe. Galvanic corrosion of a model Cu-Fe pair in chloride-containing solution was visualized with high spatial resolution by recording either line scans or 2D-images using the novel Pt/Sb multi-barrel tip.

Keywords: Scanning Electrochemical Microscopy (SECM); Microelectrode probes; pH gradients; Galvanic corrosion; Iron; Copper.

1. Introduction

Chemical imaging of reactive surfaces with high spatial resolution has become available with the introduction of scanning electrochemical microscopy (SECM) [1-3]. SECM is based on the reaction that occurs at a mobile microelectrode tip scanned in close vicinity of a surface immersed in an electrolyte solution [4,5]. A faradaic current is measured at the tip due to the redox conversion of an oxidizable/reducible species present in the solution (usually called the mediator), and it depends strongly on the tip-sample separation and the redox activity of the solid/liquid interface [4]. Therefore, by scanning the tip over a given surface, an image of the surface can be generated that contains information concerning reactions that take place either in the solution space between the tip and the sample or on the surface of the scanned sample. As result, the SECM is a unique near-field scanning technique for the investigation of chemical and electrochemical activities in heterogeneous systems such as the greatly localized corrosion processes taking place on metal surfaces in aqueous solutions [6,7]. In fact, this technique is currently employed to locate and monitor the active corroding sites and give details of the localized currents and compositional changes by scanning the surface and mapping ionic current issuing from the corroding sites and their associated concentration changes in pH, dissolved metal ions, of bulk solution anion, and dissolved oxygen [8-11].

The SECM can be used in a variety of ways, which can be broadly classified into amperometric and potentiometric modes, depending on the type of the sensing probe, namely an ultramicroelectrode (UME) and an ion-selective microelectrode, respectively [12]. Because the corroding metal usually involves local changes in ionic concentrations, as they produce M^{z+} at the anodic sites transferred under diffusion control, the system can be studied by amperometric SECM. This feature has been exploited to image the activation of precursor sites for pit generation [13,14], the conversion of specific metal cations for the visualization of metastable pits on austenitic steel [15], and the detection of metal dissolution either from inclusions in alloys [16,17], or from defects in polymer-coated metals [18]. Additionally, in a neutral aqueous media, the reaction of dissolved oxygen from the electrolyte at the cathodic areas may be analyzed through the monitoring of the subsequent depletion of oxygen content in the solution volume adjacent to the cathodic sites [19,20]. However, for the detection of concentration distributions in certain corroding samples, especially for metals with

sufficiently negative redox potentials in aqueous environments, the use of Pt microelectrodes is limited by the onset of oxygen reduction and hydrogen evolution reactions [21]**.** In addition, Pt microelectrodes are not able to detect pH variations, though the corrosion processes are associated with pH changes as the result of both the hydrolysis of the anodically-oxidized metal, and the cathodic consumption of oxygen or H^+ ions, thus local pH changes are important traits of a corroding system. Though scarcely applied, these physicochemical parameters may be studied using ion-selective microelectrodes (ISME) as tips. In this case, the SECM is operated in the potentiometric mode, which gives greater chemical selectivity [22]. In this respect, the applicability of Zn^{2+} [23,24] and Mg^{2+} ion-selective microelectrodes [25,26] with SECM has been established. On the other hand, the monitoring of concentration distributions of these two metal ions, namely Zn^{2+} [27] and Mg^{2+} [28,29], has also been achieved using the scanning ion-selective electrode technique (SIET), whereas an ion selective microelectrode for pH measurements in corrosion problems was recently employed with this technique [30,31]. Yet, the measurement of pH distributions with the SECM are usually performed using Sb/Sb_2O_3 microelectrodes instead, because they can operate as dual amperometric/potentiometric probes by adequate selection of the potential applied to them [32]. This feature allows precise positioning of the tip with respect to the substrate using the procedures available in SECM [33].

Despite the advantageous characteristics of SECM for the investigation of corroding surfaces, the analysis of the electrochemical response recorded at the tip is often ambiguous, due to either the combination of topographical and chemical changes, or the simultaneous contribution of more than one redox active species to the current flowing at the tip. Next, the use of different operation modes requires the exchange of the scanning probe between measurements, a procedure that greatly hinders accurate control of both the tip-substrate distance and the imaging of the same features on the surface. The latter is especially relevant in corrosion researches due to the high reactivity of the surface that originates topographical and chemical changes during the process. To overcome these limitations, novel probes must be designed for multifunction operation in SECM.

In this context, the multi-channel and multi-barrel electrodes employed in life sciences, particularly in iontophoresis [34,35] and for neuroanalytical purposes [36,37], appear an attractive option. Most interestingly, ion selective multi-barrel electrodes have been already employed to measure K^+ and pH in barley root cells [38], and K^+ and Na^+

in clinical research [39]. Yet, multi-barreled SECM microelectrodes comprising an amperometric and potentiometric channels were developed two decades ago [40], making use of gallium to overcome the difficulties on sealing a Pt or C wire in glass; whereas dual-barrel micropipettes were recently applied in scanning ion conductance microscopy (SICM) for the simultaneous imaging of topography and pH profiles [41,42]. However, to the best of our knowledge, the microelectrochemical characterization of corroding surfaces with amperometric probes in combination with potentiometric sensors in a single electrode has not been reported.

In this work we present a double-barrel microelectrode design to be employed in scanning electrochemical microscopy as combined probe for either potentiometric/amperometric operation or the simultaneous potentiometric monitoring of various chemical species. The suitability of combined amperometric/potentiometric operation in SECM to the monitoring of corroding systems in a single experiment was tested on a model system, the galvanic corrosion of an iron-copper pair immersed in sodium chloride solution, a system previously characterized using conventional single microelectrode tips [43], thus requiring separate experiments to perform the amperometric and potentiometric characterizations of the system due to probe replacement and sample surface preparation.

1. Experimental

2.1. Chemicals, materials

Antimony and platinum disc microelectrodes were fabricated using high purity antimony in powder presentation (266329, Aldrich), or 99.9% purity platinum wire of 12.5 μm diameter (Goodfellow, Cambridge, United Kingdom). Micropipettes were obtained by pulling borosilicate capillaries (outer diameter Ø = 1.5 mm, inner dia. Ø = 1.0 mm), purchased from Hilgenberg GmbH (Malsfeld, Germany), with a Narishige PE-2 pipette puller (Tokyo, Japan).

Analytical grade reagents and ultra-pure water purified using a Milli-Q system (Millipore, Billerica, MA, USA) were employed to prepare all the solutions. Tests were conducted in NaCl solutions, naturally aerated, at ambient temperature. Ferrocene-methanol (Aldrich) was used as mediator in feedback experiments.

In this work, we monitored the corrosion reactions occurring at an iron-copper galvanic pair. Iron and copper wires (dia. 0.7 mm) supplied by Goodfellow (Cambridge,

United Kingdom) were mounted into an Epofix (Struers, Ballerup, Denmark) resin sleeve, in order that their cross sections formed the testing sample. Galvanic connection between the two metals could be electrically performed at the back of the mount. The samples, after curing for 12 hours at room temperature, were abraded with silicon carbide paper down to 4000 grit, and subsequently polished with Micropolish II Alumina Suspension of 1 and of 0.3 μm particle size (Buehler, Lake Bluff, IL, USA). The resulting surfaces were thoroughly rinsed with Millipore deionized water, dried with ethanol and finally surrounded laterally by sellotape, thus creating a container for the test electrolyte solution.

2.2. Instruments

The SECM equipment used in this work was built by Sensolytics (Bochum, Germany), using an Autolab (Metrohm Autolab, Utrecht, The Netherlands) electrochemical interface, all controlled with a personal computer. For the potentiometric operation, using the antimony-based pH sensitive tips microelectrode, a homemade voltage follower based on a 10^{12} Ω input impedance operational amplifier was interconnected between the cell and the potentiometric input of the electrochemical interface. Additionally, a Dropsens μStat400 bipotentiostat (Llanera, Asturias, Spain) was employed in the amperometric measurements with platinum microelectrodes. The electrochemical cell was completed with an Ag/AgCl/(3.5 M) KCl electrode as reference (E_0 = +0.197 V vs. NHE), and a Pt plate as counter electrode (approximate area 0.72 cm^2). All potential values are referred to the Ag/AgCl/(3.5 M) KCl electrode. A video camera was used to assist positioning of the tip close to the surface, as well as to obtain micrographs of the investigated system in situ.

2. Results and discussion

3.1. Fabrication and characterization of the double-barrel microelectrode probe assembly

A novel double-barrel antimony and platinum microelectrode assembly was developed. The design had to account for the different surface preparation of the metal discs of each metal as result of their different operation as SECM probe. Namely, platinum disc microelectrodes used in amperometric operation are usually employed

after careful grinding and polishing in order to obtain a clean and reproducible surface, but polishing would modify the oxide layer formed on the antimony surface that exhibits potentiometric response to pH changes. On the other hand, prior to operation, the antimony microelectrode must be calibrated in a range of acidic and alkaline buffer solutions, which can eventually contaminate the surface of the platinum electrode. In order to overcome these difficulties, a new double-barrel design was developed as sketched in Figure 1. It is based in the fabrication of the pH antimony microelectrode as a separate removable component that will be inserted into the lumen of the one of the barrels. To this end, a thinner glass capillary is fabricated in addition to the double-barrel glass micropipette. In this arrangement, the two microelectrode disks can be physically separated for either the calibration of the antimony electrode or the surface preparation process of the Pt electrode, whereas the antimony-based electrode can be introduced back into the lumen of the corresponding micropipette in the double-barrel assembly for the visualization of the corrosion system to be investigated.

Double-barrel glass micropipette arrangements were pulled out together from two borosilicate capillaries. Subsequently, the platinum disc microelectrode was fabricated by inserting approximately 1.5-2 cm long portion of a 12.5 μm dia. wire into one of the barrel capillaries, and heating the end to solder the metal to the glass. The electric contact was attained by welding a copper wire to the other end of the Pt wire, and then fixing the weld inside the glass pipette by means of silver-epoxy glue. The active Pt disc surface was first abraded using a sequence of grinding emery papers up to 4000 grit, and subsequently polished with 1, 0.3, and 0.05 μm alumina slurries in ethanolic suspension. The performance of the Pt disc was tested by cyclic voltammetry in 1 mM NaCl + 0.56 mM ferrocene-methanol solution, using Ag/AgCl/(3.5 M) KCl electrode as reference and Pt plate as counter electrodes. Ferrocene-methanol was added to provide a model reversible one-electron redox process. A cyclic voltammogram recorded at the Pt microelectrode in the Pt/Sb double-barrel electrode assembly is depicted in Figure 2. It shows the typical behavior of a Pt microelectrode of approximate diameter 12.5 μm. Measurements were always done in triplicate, showing good reproducibility due to the well defined active area and controlled tip geometry.

The removable antimony microelectrode was fabricated by melting a few grams of antimony powder that was introduced into a glass capillary with a syringe. Using metallic tweezers and a roaring flame of a Bunsen, thinner capillaries filled with

antimony were obtained. The pulling step could be eventually repeated a few times to produce antimony fibers in micron or even submicron range. The thin capillaries were checked under optical microscope and the parts without air bubbles were selected. One of these pieces would be inserted and fixed at the end of the tip of the electrode body. The electric contact between a copper wire and the antimony was attained with liquid mercury. In this work, antimony fibers of approximately 15 μm dia. were employed. Slight differences in diameter of the Sb active areas resulted in different spatial resolution, although the potential response towards pH did not vary with the exposed area, as expected for intensive magnitudes. The microelectrodes were subsequently calibrated in pH buffers covering the range between pH=11 and pH=4. Sometimes, it was necessary to renew the Sb_2O_3 layer on the surface of the antimony electrode. This was performed by either soaking the microelectrode in pH=4 buffer solution for a few minutes, or under electrochemical polarization at 0.0 V vs. Ag/AgCl/(3.5 M) KCl for 1 minute. A typical calibration curve for the pH response of the antimony-based microelectrode is shown in Figure 3. A good linear relationship with slope amounting -50.5 mV $decade^{-1}$ was found. Though a sub-Nernstian type response was obtained for this pH microsensor, instead of the -59 mV $decade^{-1}$ theoretical value, this behavior is not uncommon for the Sb/Sb_2O_3 surfaces [32,33].

3.2. Combined amperometric/potentiometric SECM characterization of an iron-copper galvanic pair

Combined amperometric/potentiometric SECM operation for the characterization of a galvanic corrosion process using the new double-barrel microelectrode probes was explored using an iron-copper sample immersed in naturally aerated 10 mM NaCl aqueous solution at ambient temperature. Greater driving force towards corrosion is experienced by iron in this environment when the two metals are not galvanically coupled. The onset of corrosion on the surface of iron leads to the formation of a rust deposit at the cathodic areas developed on this metal, a feature observed with the videocamera after only 3 hours exposure (see Figure 4A). When the same experiment is performed with the two metals electrically-connected at the rear of the sample, the anodic reaction occurs on the surface of iron, whereas copper is the cathode. Furthermore, the rate of the anodic reaction on the iron surface is higher when galvanically-coupled to copper than in the case of the spontaneous dissolution of the disconnected metal, as it can be observed in the micrograph of Figure 4B.

Visualization of the corroding system was first attempted by recording scan lines taken across the center of the two metal wires while electrically-connected at the rear of the mould, in order to record both amperometric and potentiometric data during the same scan. The vertical tip-sample distance was set to 20 μm. Location of the surface was first established by gently approaching the double-barrel electrode to the sample and then lifting it up for the desired distance, confirming that both microdisks were touching their respective reflections at the metal surface at the same vertical position. Besides, approach curves were done over the insulating resin with the Pt electrode registering the electro-reduction of the dissolved oxygen [18], in order to confirm the location of the surface.

The potentiometric response of the antimony-based microelectrode is shown in Figure 5, closely matching previous reports for this system [43]. The cathodic reaction consumes oxygen and produces OH^- ions according to eqn. (1), which originates the pH increase observed above the copper wire with the antimony microelectrode.

$$O_2 + 2H_2O + 4e^- \rightarrow 4OH^- \quad (1)$$

On the other hand, iron oxidizes to iron (II) in the anodic reaction according to eqn. (2), and the hydrolysis of the dissolved metal ions releases hydrogen ions:

$$Fe \rightarrow Fe^{2+} + 2e^- \quad (2)$$

$$Fe^{2+} + nH_2O \rightarrow Fe(OH)_n^{2-n} + nH^+ \quad (3)$$

The latter produces the local acidification of the electrolyte in the close proximity of the iron wire.

Indeed, all these pH variations are clearly displayed in the scan line of Figure 5. It must be noticed that this measurement was carried out while no potential was applied to the Pt electrode in the double-barrel probe. In separate experiments it was investigated the eventual cross-talking between the microelectrodes though separate instruments were employed for recording the potentiometric and amperometric responses of the dual probe. This was done by recording voltammetric signals at different potential values applied to the Pt microelectrode, with the result that variations in the open circuit potential of the Sb electrode occurred. These variations accounted for more than 100 mV (i.e., two orders of magnitude) and occurred abruptly once the platinum electrode was biased. Although simultaneous amperometric-potentiometric measurements have been reported to be feasible signaling alternating current (AC) signals when applying an

AC potential to the unbiased amperometric sensor of dual-barrel SICM-pH probes [41,42], the herein encountered cross-talk effect between the polarized Pt and the pH-sensitive Sb-based electrode prevented us from simultaneously collecting information from both channels. Thus, adequate electronic circuitry must still be developed in order to enable simultaneous OCP-amperometric measurements in the same cell with the dual electrode described herein. Alternately, the measurements reported in this contribution using the Pt-Sb double barrel electrode were quasi-simultaneous, that is, the same scan line was recorded two times sequentially, the first for the potentiometric measurement with the antimony microelectrode, and the second with the amperometric operation of the platinum disc.

By adequate selection of the potential value applied to the platinum disc microelectrode employed as amperometric sensor, various species participating in the corrosion reaction could also be monitored with chemical selectivity. In this way, the soluble Fe(II) species generated at the local anodes formed on the iron wire were collected at the Pt disc when polarized at +0.50 V vs. Ag/AgCl/(3.5 M) KCl through their oxidation to Fe(III) [15,44]. Due to the oxidation of iron (II) at the platinum disc, an increase of the faradaic current recorded at the tip should be observed when passing over the corroding iron specimen. This is actually the behavior described by the scan line depicted in Figure 6. A clear oxidation peak is always observed above the background current signal when the probe travels above the iron wire. That is, the platinum microelectrode in the double-barrel probe is collecting the metal ions generated in the corroding sample. Since these measurements were conducted after 3 hours immersion in the electrolyte to allow for the onset of the galvanic corrosion process, there is already some background Fe(II) concentration in the small volume electrolyte resulting from the diffusion of the metal ions released from the surface prior to recording the scan line given in Figure 6. It must also be noticed that this background current for Fe(II) dissolution is basically the same independently of the location on the sample beyond the iron wire, namely above the resin and above the copper wire.

On the other hand, the cathodic reaction occurring at the copper specimen is the consumption of dissolved oxygen in the electrolyte. This reduction reaction involves 4 electrons as described by equation (1). The local depletion of dissolved oxygen concentration in the electrolyte adjacent to the corroding sample due to its consumption at the cathodic sites can be also amperometrically imaged with the platinum microelectrode cathodically polarized, as it was previously reported [18,44]. In the bulk

of the electrolyte, oxygen concentration can be assumed to remain constant, but in the proximity of the copper sample it is smaller due to its reduction consuming the electrons released by the corroding metal. This phenomenon is known as the redox competition mode of SECM [19,45]. The scan line shown in Figure 7 evidences that oxygen is consumed over the copper wire, actually leading to its (almost) complete consumption as indicated by the monitoring of faradaic currents very close to zero over this metal. But quite a similar behavior is frequently observed above the iron wire, which indicates that both the cathodic and the anodic half-cell reactions can simultaneously occur over the less noble metal. Indeed, the electrons released by the dissolving Fe(II) ions must travel to the corresponding cathodic sites in order to be transferred to the oxygen molecule. Provided the anodic reaction is not homogeneously distributed over the iron wire, the iron surface surrounding the actual anodic sites can act as the location for the electron exchange to the dissolved oxygen molecules, most particularly when oxygen depletion over the copper wire has been almost complete in this case as observed in Figure 7. The quasi-simultaneous amperometric/potentiometric operation of the double-barrel probe has allowed for the cathodic reaction in the galvanic corrosion of a Cu-Fe pair to be imaged with high resolution. The simultaneous occurrence of the cathodic reaction around the localized anodic sites developed on the less noble metal was already described for a different galvanic couple, namely Fe-Zn, though in separate experiments [46,47]. In addition, the presence of corrosion products on the iron, as it is observed in Figure 4, may also contribute to the decrease of the tip current because the diffusion of oxygen from bulk solution towards the sensitive tip becomes hindered. However, further experiments confirmed that the electrochemical reaction of the oxygen was indeed taking place on iron, as it will be discussed below.

It is well known that the oxygen reduction reaction on non-noble metals usually consists of at least two redox steps involving the generation of hydrogen peroxide, according to equation (4):

$$O_2 + 2H_2O + 2e^- \rightarrow H_2O_2 + 2OH^- \qquad (4)$$

Thus, hydrogen peroxide can be detected at the platinum electrode when polarized at 0.0 V vs. Ag/AgCl/(3.5 M) KCl [20]. Yet, it must be noticed that at this potential value, the reduction of any Fe^{3+} species can also occur [20]. Figure 8 shows an oxidation peak above the copper disk that distinctly shows the signal of hydrogen-peroxide, an intermediate of the oxygen reduction reaction. On the other hand, above the iron wire

the cathodic current increased below the baseline, which indicates the reduction of Fe^{3+}. The origin of Fe^{3+} ionic species distributed around the iron sample is an indirect evidence of the distribution of anodic and cathodic sites on Fe, the latter eventually releasing OH^- ions that react homogeneously in the solution phase with a fraction of the dissolved Fe^{2+} ions from the anodic sites [15]. The reduction signal is not centered above the iron wire but rather shifted to the left side, that is, closer to the copper wire, which is the main source for both OH^- and H_2O_2 species as result of the cathodic half-cell reaction. Again, the consumption of oxygen was detected above the copper wire through the corresponding decrease in current. Despite some poor resolution, relatively bigger corrosion activity can be observed at the edge of the iron disc.

After completing the amperometric measurement and switching off the potential applied to the Pt electrode, potentiometric array scans were performed using the antimony microelectrode in the double-barrel probe. The scan was recorded in meander mode over a 2200 μm × 1000 μm area, with 50 μm distance between the measured points in a given line along the *X* axis (the diameters of both the copper and the iron wires were 0.7 mm), and the tip was shifted 100 μm along the *Y* axis after completing every *X* line. In the meander algorithm, the tip scans a rectangular area by executing a series of line scans. The scanning direction along the *X* axis alternates from line to line. That is, as the probe reaches the last rastered point of the line, for instance in the *X*+ direction, and the corresponding measurement of the probe signal at that given point is completed, the tip moves one step in the *Y* direction, and subsequently continues the scan along the opposite direction in the *X* axis (i.e., *X*- direction). In this way, the experimental data acquisition of the complete 2D map takes approximately two and a half hours using the meander mode which causes some distortion of the image. In our laboratory, extensive studies are currently carried out in order to improve the sensitivity as well as the collection rate of the data by employing deconvolution procedures [48,49].

Figure 9 shows the pH distribution over the corroding galvanic Fe-Cu couple obtained using this procedure, which better reveals the distributed nature of the dynamic corrosive attack. The image, recorded using the meander mode, shows significant distortion due to the high-speed acquisition despite application of the deconvolution techniques, although the actual spatial pH distribution can be properly observed. Almost homogeneous alkalization of the electrolyte occurs above the copper wire, indicating that all the surface of the metal is active towards the reduction of oxygen. The cathodic

activity occurs over the complete copper surface, though it is more intense at its center (within a concentric area of ca. 350 μm diameter), and the electrolytic environment only becomes neutral at the very edge of the copper specimen that is closer to the anodic region on the other metal, which produces local acidification.

Conversely, this anodic reaction is rather heterogeneous in nature, with anodic sites locally developing on a 150-200 μm diameter portion of the exposed iron surface, as indicated by the more acidic locations in the map. In addition, since the acidic electrolyte generated over the iron diffuses towards the surrounding environment, the solution becomes more acidic at the right side of the iron, in contrast to the intermediate region between the metal specimens where acid-alkali neutralization occurs. The acquisition of the scan in meander mode indirectly reveals that this observation is not caused by the convection caused by the tip movement, since in such case the acidification at the right side of the iron would be only observed for the linear scans recorded from left to right. Finally, the spatial resolution of the scan was set to 50 μm steps in order to accelerate the data acquisition in the highly dynamic system, and such resolution seems to provide satisfactory results for the visualization of the heterogeneous surface response.

Finally, the heterogeneous nature of the corrosion process occurring on the Fe wire could also be shown by recording the amperometric signal for oxygen consumption when the experiment was performed with the disconnected two metals, i.e., spontaneously corroding in the test electrolyte according to their individual corrosion rates. From the inspection of Figure 10, which illustrates the typical trend of the response obtained over freely corroding metals, it is observed that oxygen consumption occurs at a greater extent above the iron wire, thus evidencing that iron corrodes faster in this electrolyte. More interestingly, oxygen consumption over iron displays two peaks instead of only one for copper. This is an indication that the anodic sites are located more to the centre of the iron sample, and they are surrounded by a greater cathodic area whereas oxygen reduction takes place consuming the electrons released by iron ions. In a scan line, this greater cathodic area developed around the more central anodic sites gives rise to the two oxygen consumption peaks over iron seen in Figure 10.

3. Conclusions

Quasi-simultaneous combined amperometric/potentiometric operation of SECM using a new double-barrel Pt/Sb probe has been presented in this work. This probe is allows to use the chemical detection power of the amperometric modes with the imaging of pH distributions in the usually complex corrosion processes in situ in one single experiment. In this way, neither replacement of the sensing probe nor modification of the measuring control instrumentation is required between the measurements, effectively allowing for the sequential recording of various signals in the same run. This new procedure allows a more precise characterization of localized domains with higher informative power under real corrosion conditions by allowing corrosion currents related to the conversion of different chemical species to be spatially corresponded to pH changes in the adjacent electrolyte. These features have been satisfactorily employed to monitor the physicochemical characteristics of the galvanic corrosion of a model iron-copper couple. This clearly demonstrates the advantages of the new experimental arrangement in quantitative characterization of corrosion reactions.

Acknowledgments

Financial support by the Spanish Ministry of Economy and Competitiveness (MINECO, Madrid) and the European Regional Development Fund, under grants CTQ2012-36787 and CTQ2016-80522 is gratefully acknowledged. D. Filotás acknowledges a 2-month mobility grant to the University of La Laguna funded by the ERASMUS+ programme. B.M. Fernández-Pérez is grateful for the financial support of Obra Social La Caixa-Fundación Cajacanarias (Beca de Investigación para Postgraduados de la Universidad de La Laguna).

References

1. R.C. Engstrom, M. Weber, D.J. Wunder, R. Burgess, S. Winquist, Measurements within the diffusion layer using a microelectrode probe, Anal. Chem. 58 (1986) 844-848.
2. J.Y. Liu, F.R.F. Fan, C.W. Lin, A.J. Bard, Scanning electrochemical and tunneling ultramicroelectrode microscope for high-resolution examination of electrode surfaces in solution, J. Am. Chem. Soc. 108 (1986) 3838-3839.

3. A.J. Bard, F.R.F. Fan, J. Kwak, O. Lev, Scanning electrochemical microscopy. Introduction and principles, Anal. Chem. 61 (1989) 132-138.
4. J. Kwak, A.J. Bard, Scanning electrochemical microscopy. Theory of the feedback mode, Anal. Chem. 61 (1989) 1221-1227.
5. A.J. Bard, G. Denuault, C. Lee, D. Mandler, D.O. Wipf, Scanning electrochemical microscopy: A new technique for the characterization and modification of surfaces, Acc. Chem. Res. 23 (1990) 357-363.
6. P. Marcus, F. Mansfeld (Eds.), Analytical Methods in Corrosion Science and Engineering. CRC Press, Boca Raton (FL, USA), 2006.
7. R. Oltra, V. Maurice, R. Akid, P. Marcus (Eds.), Local Probe Techniques for Corrosion Research. Woodhead Publishing, Cambridge (England), 2007.
8. L. Niu, Y. Yin, W. Guo, M. Lu, R. Qin, S. Chen, Application of scanning electrochemical microscope in the study of corrosion of metals, J. Mater. Sci. 44 (2009) 4511–4521.
9. Y. González-García, J.J. Santana, J. González-Guzmán, J. Izquierdo, S. González, R.M. Souto, Scanning electrochemical microscopy for the investigation of localized degradation processes in coated metals, Prog. Org. Coat. 69 (2010) 110-117.
10. H. Luo, C. Dong, S. Gao, C. Du, K. Xiao, X. Li, Sensing application in the precursor region of localized corrosion by scanning electrochemical microscopy, RSC Adv. 4 (2014) 56582-56595.
11. M.B. Jensen, D.E. Tallman, Application of SECM to Corrosion Studies. In: Electroanalytical Chemistry: A Series of Advances, Vol. 24, A.J. Bard, C. Zoski (Eds.). CRC Press, Boca Raton (FL, USA), 2012, pp. 171-286.
12. A.J. Bard, M.V. Mirkin (Eds.), Scanning Electrochemical Microscopy, 2nd edition. CRC Press, Boca Raton (FL, USA), 2012.
13. N. Casillas, S.J. Charlebois, W.H. Smyrl, H.S. White, Scanning electrochemical microscopy of precursor sites for pitting corrosion on titanium, J. Electrochem. Soc. 140 (1993) L142-L145.
14. Y. Zhu, D.E. Williams, Scanning electrochemical microscopic observation of a precursor state to pitting corrosion of stainless steel, J. Electrochem. Soc. 144 (1997) L43-L45.
15. Y. González-García, G.T. Burstein, S. González, R.M. Souto, Imaging metastable pits on austenitic stainless steel in situ at the open-circuit corrosion potential, Electrochem. Commun. 6 (2004) 637-642.

16. C.H. Paik, H.S. White, R.C. Alkire, Scanning electrochemical microscopy detection of dissolved sulfur species from inclusions in stainless steel, J. Electrochem. Soc. 147 (2000) 4120-4124.
17. M.B. Jensen, A. Guerard, D.E. Tallman, G.P. Bierwagen, Studies of electron transfer at aluminum alloy surfaces by scanning electrochemical microscopy, J. Electrochem. Soc. 155 (2008) C324-C332.
18. R.M. Souto, Y. González-García, S. González, In situ monitoring of electroactive species by using the scanning electrochemical microscope. Application to the investigation of degradation processes at defective coated metals, Corros. Sci. 47 (2005) 3312-3323.
19. J.J. Santana, J. González-Guzmán, L. Fernández-Mérida, S. González, R.M. Souto, Visualization of local degradation processes in coated metals by means of scanning electrochemical microscopy in the redox competition mode, Electrochim. Acta 55 (2010) 4488-4494.
20. S. González, J.J. Santana, Y. González-García, L. Fernández-Mérida, R.M. Souto, Scanning electrochemical microscopy for the investigation of localized degradation processes in coated metals: Effect of oxygen, Corros. Sci. 53 (2011) 1910-1915.
21. R.M. Souto, Y. González-García, D. Battistel, S. Daniele, In situ SECM detection of metal dissolution during zinc corrosion by means of mercury sphere-cap microelectrode tips, Chem. Eur. J. 17 (2011) 230-236.
22. K. Toth, G. Nagy, C. Wei, A.J. Bard, Novel application of potentiometric microelectrodes –Scanning potentiometric microscopy, Electroanalysis 7 (1995) 801-810.
23. Á. Varga, L. Nagy, J. Izquierdo, I. Bitter, R.M. Souto, G. Nagy, Development of solid contact micropipette Zn-ion selective electrode for corrosion studies, Anal. Lett. 44 (2011) 2876-2886.
24. J. Izquierdo, L. Nagy, Á. Varga, I. Bitter, G. Nagy, R.M. Souto, Scanning electrochemical microscopy for the investigation of corrosion processes: measurement of Zn^{2+} spatial distribution with ion selective microelectrodes, Electrochim. Acta 59 (2011) 398-403.
25. J. Izquierdo, A. Kiss, J.J. Santana, L. Nagy, I. Bitter, H.S. Isaacs, G. Nagy, R.M. Souto, Development of Mg^{2+} ion-selective microelectrodes for potentiometric scanning electrochemical microscopy monitoring of galvanic corrosion processes, J. Electrochem. Soc. 160 (2013) C451-C459.

26. R.M. Souto, A. Kiss, J. Izquierdo, L. Nagy, I. Bitter, G. Nagy, Spatially-resolved imaging of concentration distributions on corroding magnesium-based materials exposed to aqueous environments by SECM, Electrochem. Commun. 26 (2013) 25-28.
27. A.C. Bastos, M.G. Taryba, O.V. Karavai, M.L. Zheludkevich, S.V. Lamaka, M.G.S. Ferreira, Micropotentiometric mapping of local distributions of Zn^{2+} relevant to corrosion studies, Electrochem. Commun. 12 (2010) 394-397.
28. S.V. Lamaka, O.V. Karavai, A.C. Bastos, M.L. Zheludkevich, M.G.S. Ferreira, Monitoring local spatial distribution of Mg^{2+}, pH and ionic currents, Electrochem. Commun. 10 (2008) 259-262.
29. O.V. Karavai, A.C. Bastos, M.L. Zheludkevich, M.G. Taryba, S.V. Lamaka, M.G.S. Ferreira, Localized electrochemical study of corrosion inhibition in microdefects on coated AZ31 magnesium alloy, Electrochimica Acta 55 (2010) 5401-5406.
30. S.V. Lamaka, M. Taryba, M.F. Montemor, H.S. Isaacs, M.G.S. Ferreira, Quasi-simultaneous measurements of ionic currents by vibrating probe and pH distribution by ion-selective microelectrode, Electrochem. Commun. 13 (2011) 20–23.
31. E.A. Zdrachek, A.G. Karotkaya, V.A. Nazarov, K.A. Andronchyk, L.S. Stanishevskii, V.V. Egorova, M.G. Taryba, D. Snihirova, M. Kopylovich, S.V. Lamaka, H^+-selective microelectrodes with optimized measuring range for corrosion studies, Sens. Actuator B-Chem. 207 (2015) 967–975.
32. B.R. Horrocks, M.V. Mirkin, D.T. Pierce, A.J. Bard, G. Nagy, K. Tóth, Scanning electrochemical microscopy. 19. Ion-selective potentiometric microscopy, Anal. Chem. 65 (1993) 1213-1224.
33. J. Izquierdo, L. Nagy, Á. Varga, J.J. Santana, G. Nagy, R.M. Souto, Spatially-resolved measurement of electrochemical activity and pH distributions in corrosion processes by scanning electrochemical microscopy using antimony microelectrode tips, Electrochim. Acta 56 (2011) 8846-8850.
34. J. Millar, M. Armstrong-James, Z.L. Kruk, Polarographic assay of iontophoretically applied dopamine and low-noise unit recording using a multibarrel carbon fibre microelectrode, Brain Res. 205 (1981) 419-424.

35. E. Ujec, E.E.O. Keller, N.K.V. Pavlík, J. Machek, Low-impedance, coaxial, ion-selective, double-barrel microelectrodes and their use in biological measurements, Bioeelectrochem. Bioener. 7 (1980) 363-369.
36. P.T. McCarthy, R. Madangopal, K.J. Otto, M.P. Rao, Titanium-based multi-channel, micro-electrode array for recording neural signals, Conf. Proc. IEEE Eng. Med. Biol. Soc. 5 (2009) 2062-2065.
37. A. Piironen, M. Weckström, M. Vähäsöyrinki, Ultrasmall and customizable multichannel electrodes for extracellular recordings, J. Neurophysiol. 105 (2011) 1416–1421.
38. D.J. Walker, S.J. Smith, A.J. Miller, Simultaneous measurement of intracellular pH and K^+ or NO_3^- in barley root cells using triplebarreled, ion-selective microelectrodes, Plant Physiol. 108 (1995) 743-751.
39. P.W. Dierkes, P. Hochstrate, W.-R. Schlue, Voltage-dependent Ca^{2+} influx into identified leech neurons, Brain Res. 746 (1997) 285-293.
40. C. Wei, A.J. Bard, I. Kapui, G. Nagy, K. Tóth, Scanning electrochemical microscopy. 32. gallium ultramicroelectrodes and their application in ion-selective probes, Anal. Chem. 68 (1996) 2651-2655.
41. C.A. Morris, C.-C. Chen, T. Ito, L.A. Baker, Local pH measurement with scanning ion conductance microscopy, J. Electrochem. Soc. 160 (2013) H430-H435.
42. B.P. Nadappuram, K. McKelvey, R. Al Botros, A.W. Colburn, P.R. Unwin, Fabrication and characterization of dual function nanoscale pH-scanning ion conductance microscopy (SICM) probes for high resolution pH mapping, Anal. Chem. 85 (2013) 8070-8074.
43. J. Izquierdo, L. Nagy, J.J. Santana, G. Nagy, R.M. Souto, A novel microelectrochemical strategy for the study of corrosion inhibitors employing the scanning vibrating electrode technique and dual potentiometric/amperometric operation in scanning electrochemical microscopy: Application to the study of the cathodic inhibition by benzotriazole of the galvanic corrosion of copper coupled to iron, Electrochim. Acta 58 (2011) 707–716.
44. A.C. Bastos, A.M. Simões, S. González, Y. González-García, R.M. Souto, Imaging concentration profiles of redox-active species in open-circuit corrosion processes with the scanning electrochemical microscope, Electrochem. Commun. 6 (2004) 1212-1215.

45. K. Eckhard, X. Chen, F. Turcu, W. Schuhmann, Redox competition mode of scanning electrochemical microscopy (RC-SECM) for visualisation of local catalytic activity, Phys. Chem. Chem. Phys. 8 (2006) 5359-5365.
46. R.M. Souto, Y. González-García, D. Battistel, S. Daniele, On the use of mercury-coated tips in scanning electrochemical microscopy to investigate galvanic corrosion processes involving zinc and iron, Corros. Sci. 55 (2012) 401-406.
47. J. Izquierdo, L. Nagy, S. González, J.J. Santana, G. Nagy, R.M. Souto, Resolution of the apparent experimental discrepancies observed between SVET and SECM for the characterization of galvanic corrosion reactions, Electrochem. Commun. 27 (2013) 50-53.
48. A. Kiss, G. Nagy, New SECM scanning algorithms for improved potentiometric imaging of circularly symmetric targets, Electrochim. Acta 119 (2014) 169–174.
49. A. Kiss, G. Nagy, Deconvolution of potentiometric SECM images recorded with high scan rate, Electrochim. Acta 163 (2015) 303-309.

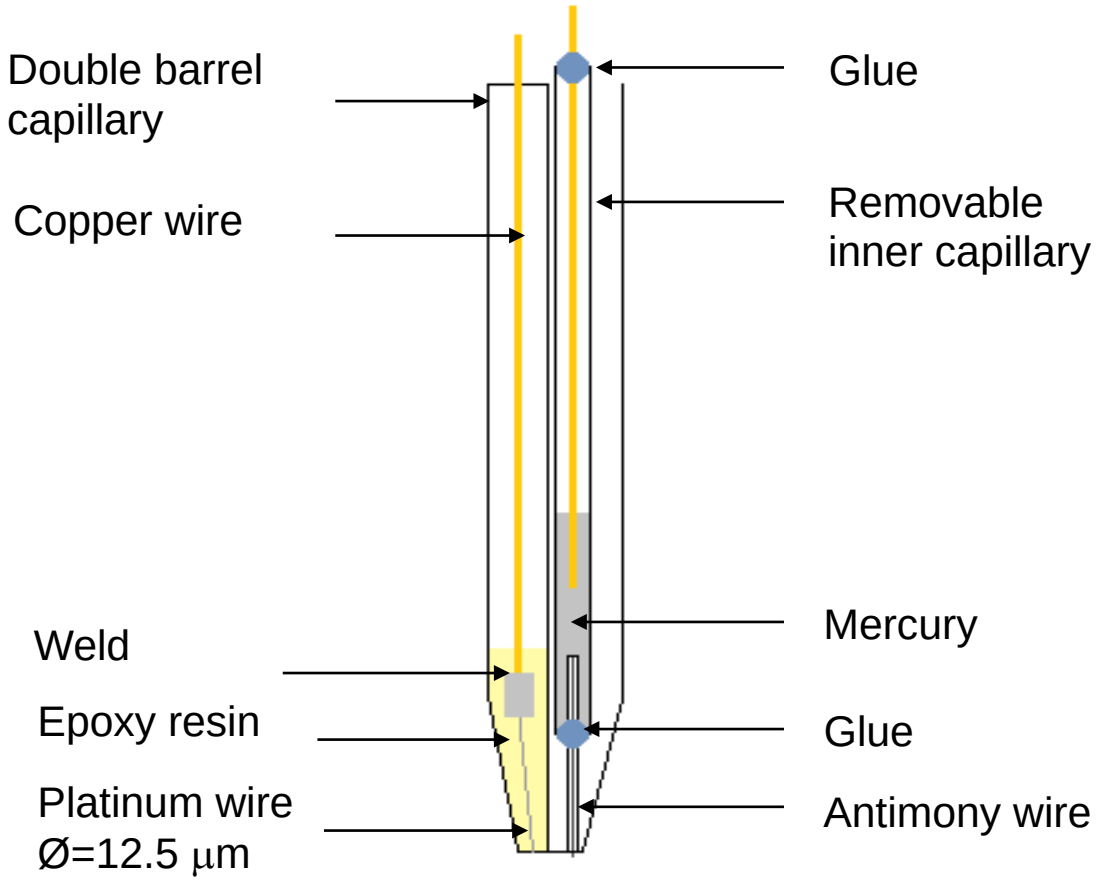

Figure 1. Sketch of the Pt/Sb double barrel double-barrel microelectrode.

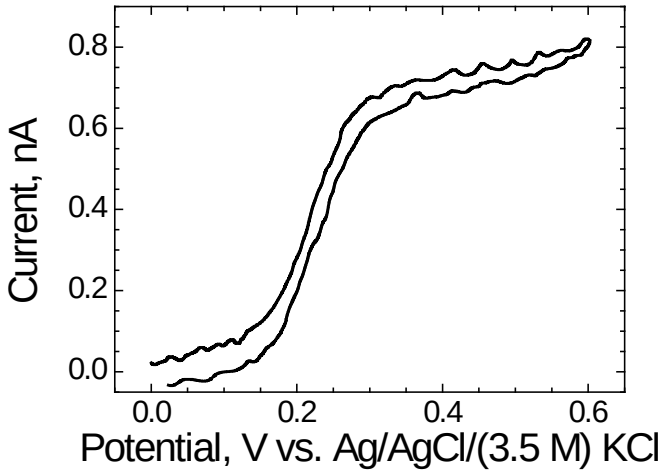

Figure 2. Cyclic voltammograms recorded with the platinum microelectrode in the double-barrel probe in naturally aerated 1 mM NaCl + 0.56 mM ferrocene-methanol. Scan rate: 0.05 V s^{-1}.

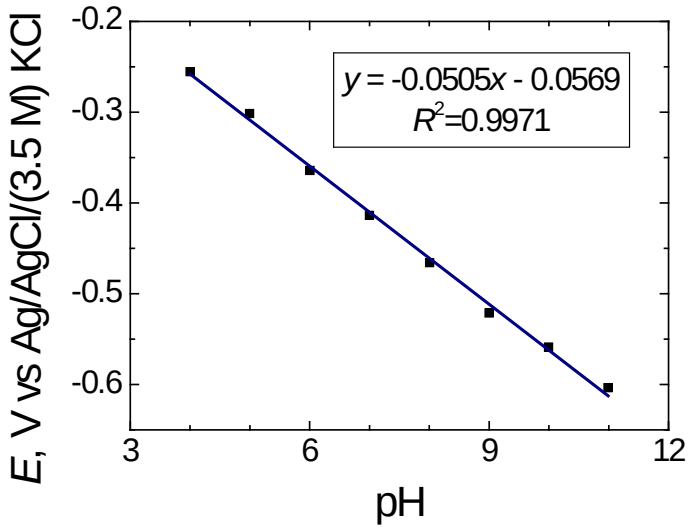

Figure 3. Calibration plot for the potential response of the antimony microelectrode in the double-barrel probe to pH.

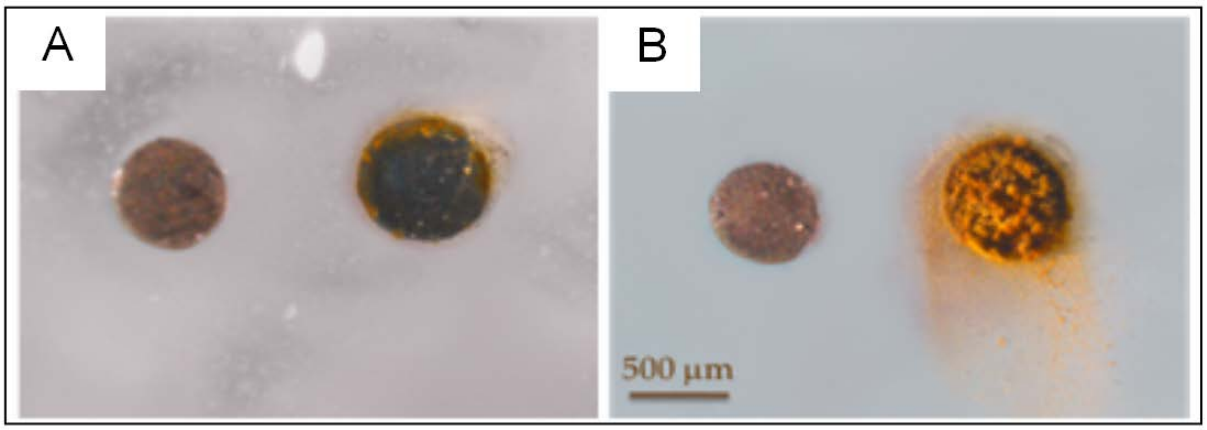

Figure 4. Optical micrographs of the Cu-Fe sample immersed in 10 mM NaCl after 3 h immersion in 10 mM NaCl solution: (A) The two metals were electrically disconnected, and (B) The two metals were electrically connected at the rear of the sample to produce a Cu-Fe galvanic couple.

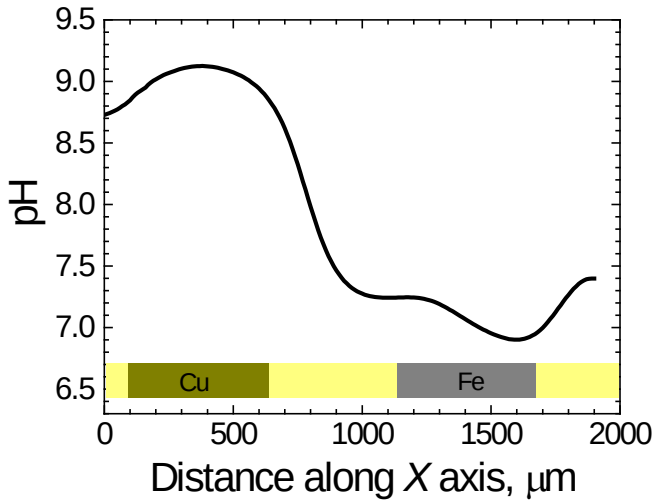

Figure 5. Potentiometric scan line of the antimony microelectrode above the copper-iron galvanic couple immersed in 10 mM NaCl.

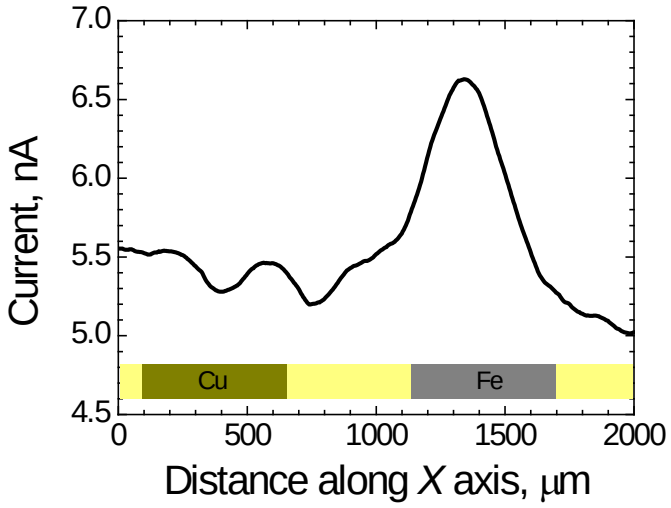

Figure 6. Scan line generated by SECM with the platinum microelectrode passing over the centers of a copper-iron galvanic couple immersed in 10 mM NaCl. SECM operation: amperometric for the oxidation of Fe^{2+}(E_{Pt} = +0.5 V vs. Ag/AgCl/(3.5 M) KCl).

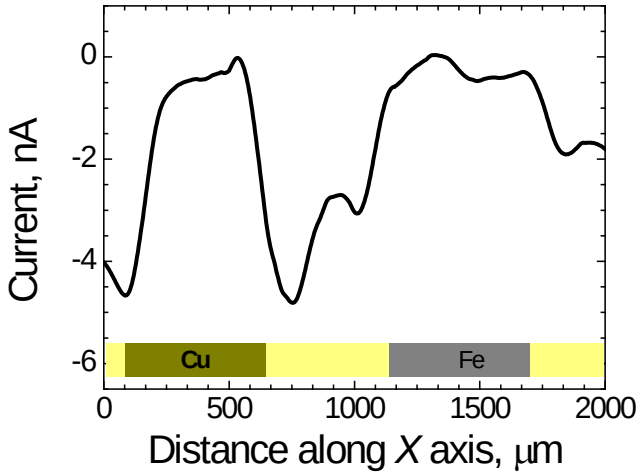

Figure 7. Scan line generated by SECM with the platinum probe passing over the centers of a copper-iron galvanic couple immersed in 10 mM NaCl. SECM operation: amperometric for the reduction of O_2 (E_{Pt} = -0.6 V vs. Ag/AgCl/(3.5 M) KCl).

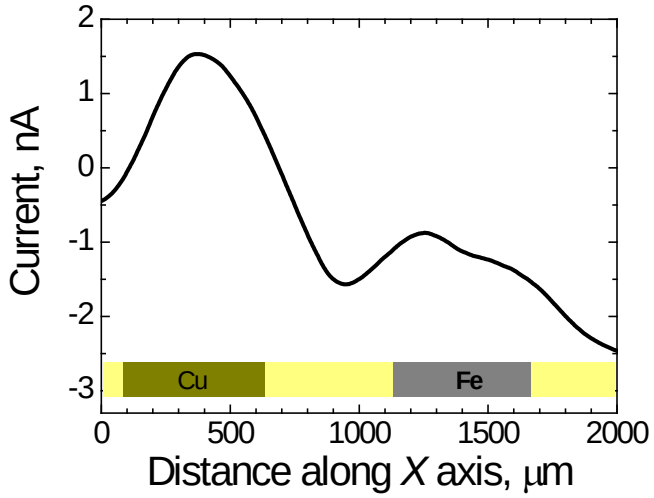

Figure 8. Scan line generated by SECM with the platinum microelectrode passing over the centers of a copper-iron galvanic couple immersed in 10 mM NaCl. SECM operation: amperometric for the both the oxidation of H_2O_2 and the reduction of Fe^{3+} (E_{Pt} = 0.0 V vs. Ag/AgCl/(3.5 M) KCl).

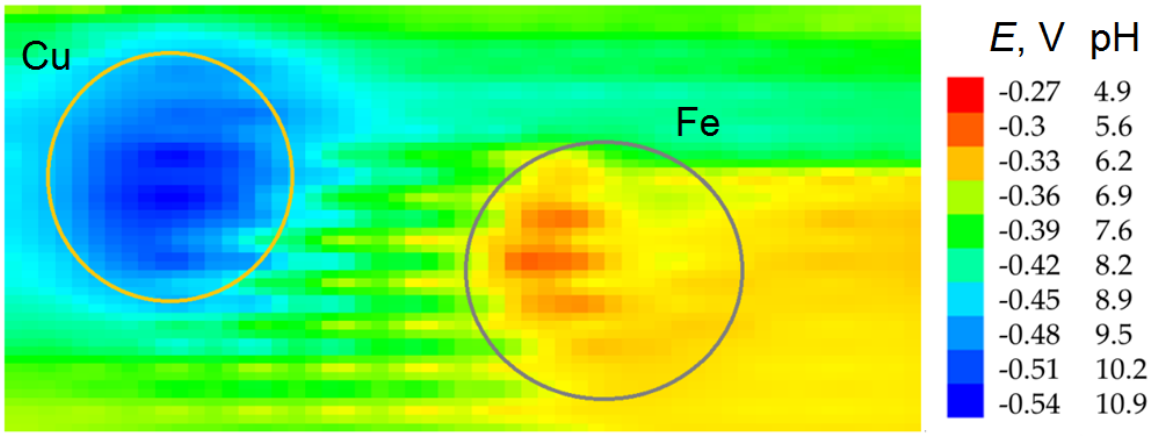

Figure 9. pH distribution above the copper-iron galvanic couple immersed in 10 mM NaCl. The image represents 2200 µm × 1000 µm in *X* and *Y* directions.

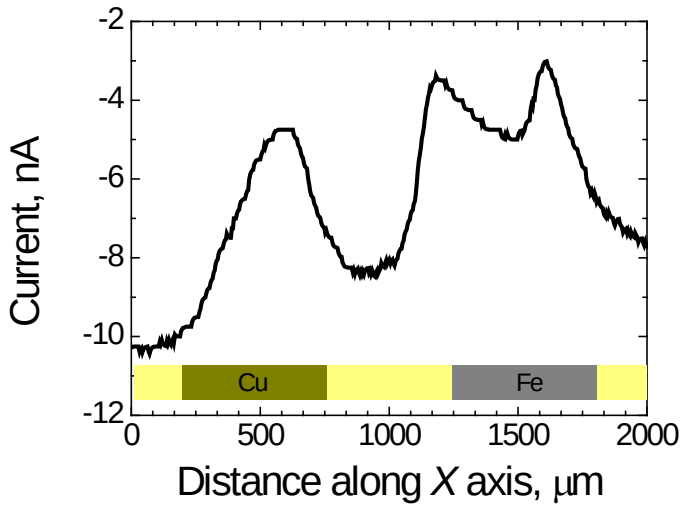

Figure 10. Scan line generated by SECM with the platinum microelectrode passing over the centers of electrically-disconnected copper and iron immersed in 10 mM NaCl. SECM operation: amperometric for the reduction of O_2 (E_{Pt} = -0.6 V vs. Ag/AgCl/(3.5 M) KCl).